HHS Public Access

Author manuscript

Inhal Toxicol. Author manuscript; available in PMC 2021 February 07.

Published in final edited form as:

Inhal Toxicol. 2020 January ; 32(1): 24–38. doi:10.1080/08958378.2020.1723746.

Mouse pulmonary dose- and time course-responses induced by exposure to nitrogen-doped multi-walled carbon nanotubes

Dale W. Porter[a], **Marlene Orandle**[a], **Peng Zheng**[b], **Nianqiang Wu**[b], **Raymond F. Hamilton Jr**[c], **Andrij Holian**[c], **Bean T. Chen**[a], **Michael Andrew**[a], **Michael G. Wolfarth**[a], **Lori Battelli**[a], **Shuji Tsuruoka**[d], **Mauricio Terrones**[d,e], **Vince Castranova**[f]

[a]National Institute for Occupational Safety and Health, Health Effects Laboratory Division, Morgantown, WV, USA

[b]Department of Mechanical & Aerospace Engineering, West Virginia University, Morgantown, WV, USA

[c]Center for Environmental Health Sciences, University of Montana, Missoula, MT, USA

[d]Research Center for Exotic Nanocarbons, Shinshu University, Nagano-shi, Japan

[e]Departments of Physics, Chemistry, Materials Science & Engineering, and Center for 2-Dimensional and Layered Materials, The Pennsylvania State University, University Park, PA, USA

[f]Department of Pharmaceutical Sciences, West Virginia University, Morgantown, WV, USA

Abstract

Objective: In this study, we compared *in vitro* and *in vivo* bioactivity of nitrogen-doped multi-walled carbon nanotubes (NDMWCNT) to MWCNT to test the hypothesis that nitrogen doping would alter bioactivity.

Materials and Methods: High-resolution transmission electron microscopy (TEM) confirmed the multilayer structure of MWCNT with an average layer distance of 0.36 nm, which was not altered by nitrogen doping: the nanomaterials had similar widths and lengths. *In vitro* studies with THP-1 cells and alveolar macrophages from C57BL/6 mice demonstrated that NDMWCNT were less cytotoxic and stimulated less IL-1β release compared to MWCNT. For *in vivo* studies, male C57BL/6J mice received a single dose of dispersion medium (DM), 2.5, 10 or 40 μg/mouse of NDMWCNT, or 40 μg/mouse of MWCNT by oropharyngeal aspiration. Animals were euthanized between 1 and 7 days post-exposure for whole lung lavage (WLL) studies.

Results and Discussion: NDMWCNT caused time- and dose-dependent pulmonary inflammation. However, it was less than that caused by MWCNT. Activation of the NLRP3 inflammasome was assessed in particle-exposed mice by determining cytokine production in WLL fluid at 1 day post-exposure. Compared to DM-exposed mice, IL-1β and IL-18 were significantly

CONTACT Dale W. Porter DPorter@cdc.gov Pathology and Physiology Research Branch, Health Effects Laboratory Division, National Institute for Occupational Safety and Health, 1095 Willowdale Road, M/S 2015, Morgantown, WV 26505, USA.

Disclosure statement

The authors declare no competing financial interests. The findings and conclusions in this report are those of the authors and do not necessarily represent the official position of the National Institute for Occupational Safety and Health, Centers for Disease Control and Prevention.

increased in MWCNT- and NDMWCNT-exposed mice, but the increase caused by NDMWCNT was less than MWCNT. At 56days post-exposure, histopathology determined lung fibrosis in MWCNT-exposed mice was greater than NDMWCNT-exposed mice.

Conclusions: These data indicate nitrogen doping of MWCNT decreases their bioactivity, as reflected with lower *in vitro* and *in vivo* toxicity inflammation and lung disease. The lower activation of the NLRP3 inflammasome may be responsible.

Keywords

Dose response; time course; multi-walled carbon nanotubes; nitrogen-doped multi-walled carbon nanotubes; NLRP3 inflammasome; lung inflammation; lung fibrosis

Introduction

The National Science Foundation estimates that by 2020 nanotechnology will have a $3 trillion impact on the global economy and employ 6 million workers in the manufacture of nanomaterial-based products, of which 2 million may be employed in the United States (WTEC Panel Report on Nanotechnology Research Directions for Societal Needs in 2020 Retrospective and Outlook 2010). Workers are at risk for exposure to carbon nanotubes during manufacturing, handling and cleanup operations (Maynard et al. 2004; Han et al. 2008; Lee et al. 2010; Dahm et al. 2012).

Previous studies from our laboratory have reported extensively on the *in vivo* toxicity of MWCNT after pharyngeal aspiration exposure. Aspiration exposure of mice to MWCNT resulted in dose- and time-dependent pulmonary inflammation and damage at lung burdens approximating feasible human occupational exposures to MWCNT (Porter et al. 2010). In addition, MWCNT exposure caused rapidly progressing fibrosis, persistent granulomous inflammation, hypertrophy and hyperplasia of bronchiolar epithelium, mucous metaplasia of the bronchiolar epithelium, and, at the highest exposures at the 56 day post-exposure time point, peribronchiolar lymphatics were dilated (Porter et al. 2010). MWCNT were also observed penetrating the pleura (Porter et al. 2010).

Surface modification of MWCNT with functional moieties is essential to extend their biological and industrial applications. For example, to apply MWCNT in biomaterials and biomedical devices, MWCNT are typically functionalized with the −COOH moiety to alter their wettability from hydrophobic to hydrophilic, which provides the active sites for further bio-conjugation (Yang et al. 2007). However, these characteristics can also potentially affect the bioactivity of MWCNT. Indeed, an *in vitro* study with primary alveolar macrophages isolated from C57Bl/J6 mice or THP-1 cells showed that functionalization of MWCNT with the −COOH group dramatically reduced their cytotoxicity and activation of the NLRP3 inflammasome (Hamilton, Wu, et al. 2013). *In vivo*, the same COOH-functionalized MWCNT caused less pulmonary inflammation, NLRP3 inflammasome activation, and pulmonary fibrosis relative to non-functionalized MWCNT after pharyngeal aspiration exposure in mice (Sager et al. 2014). These *in vivo* findings were consistent with another study, which also reported that in comparison to the native MWCNT, carboxylation of MWCNT significantly decreased pulmonary fibrosis, and extended these findings by

determining that the strongly cationic PEIMWCNT induced significantly more lung fibrosis (Li et al. 2013). However, these responses are not uniformly consistent because acid functionalization of single walled carbon nanotubes and carbon black increased their cardiopulmonary toxicity (Tong et al. 2009).

Modification of MWCNT can also be accomplished by doping them with other elements to change their intrinsic properties, but this may also alter their bioactivity. One such type of doping is with nitrogen. In this study, we compared the *in vitro* and *in vivo* bioactivity of nitrogen doped multi-walled carbon nanotubes (NDMWCNT) and compared it to MWCNT to test the hypothesis that nitrogen doping would alter bioactivity.

Materials and methods

MWCNT and NDMWCNT

MWCNT used in this study were obtained from Mitsui & Company Ltd. (MWNT-7, lot #061220-31) and were manufactured using a floating reactant catalytic chemical vapor deposition method followed by high temperature thermal treatment in argon at 2500 °C using a continuous furnace (Kim et al. 2005). NDMWCNT used in this study were a gift from Dr. Mauricio Terrones (Pennsylvania State University, University Park, PA).

Characterization of bulk MWCNT and NDMWCNT

The MWCNT and NDMWCNT were analyzed using X-ray photoelectron spectroscopy (XPS) with PHI 5000 Versa Probe system (ULVAC-PHI Inc., Chigasaki, Japan). The XPS spectra were calibrated with the reference to the C 1 s peak of carbon at 284.6 eV corresponding to carbon ring structure. The MWCNT and NDMWCNT were also observed under a high-resolution transmission electron microscope (HRTEM, JEOL, JEM 2100) at an acceleration voltage of 200 kV.

Suspension of MWCNT and NDMWCNT

Suspensions of NDMWCNT and MWCNT were prepared in dispersion medium (DM; Ca^{2+} and Mg^{2+}-free phosphate buffered saline, pH 7.4, supplemented with 5.5 mM D-glucose, 0.6 mg/ml mouse serum albumin, and 0.01 mg/ml 1,2-dipalmitoyl-sn-glycero-3-phosphocholine). DM was developed and validated by our laboratory as a vehicle for nanotoxicology studies (Porter et al. 2008). After suspension in DM, the samples were put on ice and briefly sonicated (Branson Sonifier 450, 10 W output, 50% duty cycle, 5 minutes) before use.

Sizing of NDMWCNT

Lengths and widths of NDMWCNT were determined as previously described by our laboratory (Porter et al. 2010). After suspension in DM an aliquot of NDMWCNT sample was diluted 1:1000 with dH_2O for imaging by transmission electron microscopy. A drop (approximately 0.1 ml) was deposited onto a formvar-coated copper grid and allowed to air dry. Images were photographed on a JEOL 1220 transmission electron microscope.

Zeta potential measurement of NDMWCNT

Suspensions of NDMWCNT were prepared in DM as described above. The surface charge of the NDMWCNT was measured with a Malvern Zetasizer Nano ZS instrument. For these experiments the electrophoretic mobility was converted into the zeta potential by means of the Schmolukowski relation.

Animals for in vitro *studies*

C57Bl/6 (2-months old, male) were housed in controlled environmental conditions (22 ± 2 °C; 30–40% humidity, 12-h light: 12-h dark cycle) and provided food and water ad libitum. All procedures were performed under protocols approved by the Institutional Animal Care and Use Committee of the University of Montana.

Animals for in vivo *studies*

Male C57BL/6J mice (6 weeks old) were obtained from Jackson Laboratories (Bar Harbor, ME). Mice were housed one per cage in polycarbonate isolator ventilated cages, with HEPA-filtered air and fluorescent lighting from 0700 to 1900 hours. Autoclaved Alpha-Dri virgin cellulose chips and hardwood Beta-chips were used as bedding. Mice were monitored to be free of endogenous viral pathogens, parasites, mycoplasms, Helicobacter and CAR Bacillus. Mice were maintained on Harlan Teklad Rodent Diet 7913 (Indianapolis, IN), and tap water provided ad libitum. Animals were allowed to acclimate for at least 5 days before use. All animals used in this study were housed in an AAALAC International-accredited, specific pathogen-free, environmentally controlled facility. All procedures involving animals were approved by the CDC-Morgantown Institutional Animal Care and Use Committee.

Pharyngeal aspiration exposure of mice

Mice were anesthetized with isoflurane (Abbott Laboratories, North Chicago, IL). When fully anesthetized, each mouse was positioned with its back against a slant board and suspended by the incisor teeth using a rubber band. The mouth was opened, and the tongue gently pulled aside from the oral cavity. A 50 μl aliquot of sample was pipetted at the base of the tongue, and the tongue restrained until at least 2 deep breaths were completed (but for not longer than 15 seconds). Following release of the tongue, the mouse was gently lifted off the board, placed on its left side, and monitored for recovery from anesthesia. Mice received a single dose of either DM (vehicle control), 2.5, 10, or 40 μg/mouse of NDMWCNT, or 40 μg/mouse of MWCNT.

Human THP-1 cell line culture

THP-1 cells, a human monocytic cell line obtained from ATCC, were suspended in RPMI media (Mediatech, Manassas, VA) supplemented with 10% fetal bovine serum, 50 μM β-mercapto ethanol, 1 mM sodium pyruvate, 250 ng/ml amphotericin B, and 100 U/ml penicillin and streptomycin (all supplements Media Tech, Manassas, VA), and cultured in 75 cm^2 flasks at 37 °C. The suspended cells were differentiated into macrophage-like cells by adding 150 nM vitamin D_3 (1, 25-dihydroxy, EMD Millipore, Darmstadt, Germany) for 24 hr. The semi-adherent cells were scraped with a rubber policeman in the existing media (Corning, Corning, NY) and centrifuged at 400 × *g* for 5 min. The resulting cell pellet was

re-suspended in 1 ml of complete media, and a 40 μl sample counted on a Z2 Coulter Counter (Beckman Coulter, Miami, FL). The cells were suspended at 1×10^6 cells/ml, and phorbol 12-myristate 13-acetate (5nM PMA, Sigma-Aldrich, St Louis, MO) and lipopolysacharride (10 ng/ml LPS, Sigma-Aldrich, St Louis, MO) was added to stimulate aggressive phagocytosis of the carbon nanotubes. The LPS co-stimulation was necessary to induce NF-κB translocation leading to pro-IL-1β synthesis for the NLRP3 inflammasome to cleave for IL-1β release in the transformed THP-1 model (Dostert et al. 2008; Palomaki et al. 2011). Cells, at a volume of 350 μl, were then pipetted into 1.5 ml microfuge tubes. NDMWCNT and MWCNT were added from 5 mg/ml concentrated stock suspensions to the cells. The NDMWCNT and MWCNT used a range of concentrations (0, 10, 25, 50 and 100 μg/ml). The resulting cell/particle suspension was mixed by pipette action and transferred to 96-well tissue culture plates at 100 μl per well in triplicate (100×10^3 cells/well), and cultured for an additional 24 hr in 37 °C water-jacketed CO_2 incubators (ThermoForma, Houston, TX). Viability and IL-1β levels were determined as described above with the exception of an additional viability assay for LDH (Promega, Madison, WI), which was run according to the manufacturer's protocol.

Alveolar macrophage isolation and in vitro *studies*

Mice were euthanized by IP injection of sodium pentobarbital euthanasia solution (Euthasol™) and the lungs and hearts removed. Lung lavage was performed using ice-cold PBS (pH 7.4). Lung lavage cells were isolated by centrifugation (400 × *g*, 5 min, 4 °C) and cell counts obtained using a Coulter Z2 particle counter (Beckman Coulter, Miami, FL). The collected alveolar macrophages (AM) cells were suspended in RPMI media supplemented with 10% fetal bovine serum, 0.05 mM 2-mercaptoethanol, sodium pyruvate, and supplemented with an antimycotic/antibiotic cocktail (Mediatech, Manassas, VA). Cells were suspended at 1×10^6 cells per ml and then lipopolysaccharide (LPS, Sigma-Aldrich, St Louis, MO) at 20 ng/ml added to stimulate pro-IL-1β and pro-IL-18 formation. A 100 μl sample (100,000 cells) of cells were exposed to NDMWCNT or MWCNT and incubated in 96-well plates for 24 h in 37 °C water-jacketed CO_2 incubators (ThermoForma, Houston, TX). Particle concentrations ranged from 0 to 50 μg/ml. Media was collected for IL-1β assay and determination of LDH activity. Cell viability was determined by MTS assay.

Ex vivo particle exposure and AM cell culture

C57Bl/6 mice were exposed by pharyngeal aspiration to DM, or 50 μg of MWCNT variants (MWCNT or NDMWCNT) suspended in DM (described in detail above). Following particle instillation, the mice were left for 7 days and lung cells were collected by lavage (described in detail above). The isolated cell pellet (400 × *g*, 5 min) were suspended in complete media (250 μl per single mouse lavage), cells counted as described below, and duplicate cultures of 100 μl of cells from the original volume incubated for 24 hrs with 20 ng/ml LPS to stimulate NF-κB and reveal NLRP3 inflammasome activation (similar to *in vitro* culture described above). The supernatants were collected for cytokine analysis by ELISA. The remaining 50 μl of lung cells were placed on a microscope slide by Cytospin centrifugation (300 × *g*, 5 min) and stained with a Wright/Giemsa stain in an automated Bayer slide stainer (Bayer Diagnostics). Cell differentials were determined and AM-derived cytokine levels were

adjusted to reflect the relative number of AM in the culture. Note: AM levels, typically >95%, could be as low as 50% of total lung cells in particle-exposed mice.

Toxicity assays

Cell viability was determined by MTS reagent using the CellTiter^{96} assay (Promega, Madison, WI) according to the manufacturer's protocol with the exception below. This assay used a colorimetric dye read by a colorimetric plate reader (Molecular Devices, Sunnyvale, CA). In order to avoid artifacts in the optical density values, steps were taken to remove the MTS reagent (transferring it into another plate) from the cell/particle mixture adhered to the plate bottom. The formation of bubbles was avoided and the plate was read at 490 nm.

Alternatively, LDH assays were used to confirm particle toxicity using the CellTox^{96} assay (Promega, Madison, WI) according to the manufacturer's protocol. Supernatants from *in vitro* cultures were developed for 10 min and read at 490 nm on a colorimetric plate reader (Molecular Devices, Sunnyvale, CA). Control cell cultures were lysed 30 min prior to assay establishing a total cell death value, which was used as a reference value for all other conditions.

Whole lung lavage for in vivo *studies*

At 1 and 7 days post-exposure, mice were euthanized with an ip injection of sodium pentobarbital euthanasia solution (>100 mg/kg body weight) followed by exsanguination. A tracheal cannula was inserted and whole lung lavage (WLL) performed using ice cold Ca^{2+}- and Mg^{2+}-free PBS, pH 7.4, supplemented with 5.5 mM D-glucose. Four separate lavages were performed with the first (0.6 ml) kept separate and the remaining three (1.0 ml) combined and the WLL cells isolated by centrifugation (650 × *g*, 5 min, 4 °C). An aliquot of the acellular supernatant from the first WLL (WLL fluid) was decanted and transferred to tubes for analysis of lactate dehydrogenase (LDH) and albumin. The acellular supernatants from the remaining lavage samples were decanted and discarded. WLL cells isolated from the first and subsequent lavages for the same mouse were pooled after resuspension in PBS, centrifuged a second time (650 × *g*, 5 min, 4 °C), and the supernatant decanted and discarded. The WLL cell pellet was then resuspended in PBS and placed on ice. Total WLL cell counts were obtained using a Coulter Multisizer 3 (Coulter Electronics, Hialeah, FL), and cytospin preparations of the WLL cells made using a cytocentrifuge (Shandon Elliot Cytocentrifuge, London, UK). The cytospin preparations were stained with modified Wright-Giemsa stain, and cell differentials determined by light microscopy.

Cytokine and cathepsin assays

Mouse and human IL-1β DuoSets were obtained from R&D Systems (Minneapolis, MN) and ELISA assays performed according to the manufacturer's protocol. IL-18 capture and detection antibodies were also obtained from R&D Systems. The IL-18 ELISA, although developed in-house, was run similar to R&D Systems IL-33 DuoSet ELISA with regard to timings, diluents, standard curves, and washes. Lavage fluid samples were assayed without dilution. *In vitro* media supernatants were diluted (1:5 for mouse cells, 1:100 for human cells) for optimizing the fit to the kit's standard curve. All plates were read at 450 nm and data expressed as pg/ml.

Cathepsin activity for the first WLL fluid was determined by mixing the following assay components in a 96-well plate using PBS as diluent: first WLL fluid (50 μl), 2 μg Z-LR-AMC (fluorogenic Peptide Substrate, R&D systems, Minneapolis, MN) in a total volume of 150 μl. The assays samples were incubated at 37 °C for 1 hour then fluorescence was measured using a plate reader at 380 nm excitation and 460 nm emission.

Histopathology

At 7 and 56 days post-exposure, separate sets of mice not used for BAL studies were euthanized by an overdose of pentobarbital euthanasia solution (100–300 mg/kg body weight, i.p.) followed by transection of the abdominal aorta to provide exsanguination. The lungs were rapidly removed and fixed by intratracheal perfusion with 1 ml of 10% neutral buffered formalin. Lungs were trimmed the same day, processed overnight in a tissue processor, and embedded in paraffin. Slides from the left lung lobe were prepared and stained with hematoxylin and eosin for routine morphologic assessment and with Sirius Red for evaluating fibrosis. Slides were examined in a blinded manner, and the severity of each microscopic change was scored according to the following parameters: 0 = no change, 1 = minimal, 2 = mild, 3 = moderate, 4 = marked and 5 = severe. The distribution of each change was scored as follows, 0 = no change, 1 = focal, 2 = focally extensive, 3 = multifocal, 4 = multifocal and coalescent, and 5 = diffuse. Semi-quantitative inflammation and fibrosis pathology scores were calculated as described previously (Porter et al. 2010).

Statistics

Statistical analyses for *ex vivo* and *in vitro* studies involved comparison of means using a one or two-way ANOVA followed by Dunnett's test or Bonferroni's test to compensate for increased type I error. All tests were two-tailed unless otherwise stated. Linear regression analysis was performed to determine possible predictive relationships between variables. The strength of the relationship is expressed as the coefficient of determination (r^2), indicating the proportion of variability in X explained by Y. Statistical significance was defined as a probability of type I error occurring at less than 5% ($p < 0.05$). The minimum number of experimental replications was 3. Graphics and analyses were performed on PRISM 5.0 and IBM SPSS 23.0.

For *in vivo* studies except histopathology, all outcomes yielding quantitative values were analyzed with parametric analysis of variance (ANOVA) with specific pairwise comparisons between groups. This was performed using an unequal variance model available in SAS PROC MIXED. Comparisons were made for differences in pulmonary inflammation, between one day and seven days of followup, for each treatment group (DM, MWCNT, and NDMWCNT), and comparisons between treatment groups were made for each post-exposure time. Comparisons were also made between treatments groups for activation of the NLRP3 inflammasome (cathepsin activity, IL-1β and IL-18) at one day after exposure. All statistical tests in this study are two–tailed with an $\alpha = 0.05$ significance level.

For histopathology study, because the pathology data consisted of ordinal scores, comparisons between exposure groups at each time and comparisons across time for each exposure group were accomplished using two separate oneway nonparametric analyses of

variance (ANOVAs). Exact tests were used because of the high number of tied values in the data. The nonparametric ANOVA was performed using SAS Proc NPAR1WAY with exact Wilcoxon's tests for planned pair-wise comparisons. All statistical tests were two-tailed and performed at the 0.05 significance level.

Results

Characterization of NDMWCNT

Figures 1 and 2 show the TEM and HRTEM images obtained from MWCNT and NDMWCNT, respectively. The multilayer structure of the MWCNT was observed in both samples with an average layer distance of 0.36 nm. Nitrogen doping did not change the crystal structure or the layer distance. Figures 3 and 4 show the XPS spectra obtained from MWCNT and NDMWCNT, respectively. The survey scan in Figure 3 reveals that carbon was the major element contained in the MWCNT; and oxygen was barely seen in the survey scan due to its trace content. The detailed scan of C 1 score-level has confirmed that C existed mainly in the form of a graphite-like ring structure, evidenced by a single peak at 284.6 eV. The tiny tail at the higher binding energy side of this scan shows there was a trace level of carbon in the form of C–O. This was consistent with the O 1 s peak at 532.5 eV. In addition, no nitrogen (N 1 s) was observed in the MWCNT sample. The NDMWCNT sample showed similar XPS spectra as the MWCNT sample except two N 1 s peaks were present in the detailed N1s scan (Figure 4). The N 1 s peak at 400.3 eV can be ascribed to the O–C–N or the $-C-NH_2$ bond; and the N 1 s peak at 405.0 eV might be due to the oxidation of nitrogen.

NDMWCNT width and length (Figure 5) distributions were log normal, with count median length determined to be 4.73 μm (GSD 2.33) and count median width of 52.6 nm (GSD 1.44). This is similar to MWCNT, which our laboratory previously reported to have a MWCNT median length of 3.86 μm (GSD 1.94) and count mean width of 49 nm (Porter et al. 2010).

THP-1 in vitro *studies*

A human transformed macrophage-like cell line, THP-1, was used to initially evaluate the relative toxicity and IL-1β release related to NLRP3 inflammasome activation. Figure 6 (panel A) shows the concentration-dependent toxicity of the two MWCNT, as determined by MTS assay. The NDMWCNT showed negligible toxicity in this model, contrasted to MWCNT which showed significant toxicity, particularly at the highest concentrations (50 and 100 μg/ml). It should be noted that the MWCNT used in this study was more toxic relative to the MWCNT evaluated in other studies (Hamilton, Wu, et al. 2013; Hamilton, Xiang, et al. 2013). Nitrogen-doping appeared to eliminate the toxicity from this particle in this *in vitro* exposure model. Similar to toxicity, the IL-1β release shown in Figure 6 (panel B), was significantly attenuated for the NDMWCNT. There was a slight increase in IL-1β for the NDMWCNT at high concentrations, but it was about 25% of the response compared to MWCNT. Taken together, the THP-1 particle exposure model suggests that the NDMWCNT was significantly less bioactive than the MWCNT from which it was derived.

AM in vitro *studies*

Following the THP-1 experiments, similar experiments were conducted using AM isolated from C57Bl/6 mice. Pooled AM were exposed in a similar manner to MWCNT and NDMWCNT in a concentration-dependent fashion. Toxicity results are presented in Figure 7, with panels A and B being the MTS and LDH assay results, respectively. The two assays showed consistent differences between the two particles, with the NDMWCNT being less toxic than MWCNT. However, unlike the THP-1 response, the NDMWCNT showed some toxicity at the higher concentrations tested. Statistical significance between particles was only seen in the MTS assay at higher concentrations. Figure 7 (panel C) shows the IL-1β release following 24 hr culture. This result was consistent with the THP-1 finding, where MWCNT demonstrated significant IL-1β production indicating the NLRP3 inflammasome was becoming activated in AM exposed to MWCNT. The NDMWCNT did cause some IL-1β release from AM, but it was significantly lower than MWCNT at 10 and 25 μg/ml concentrations. Combined with the THP-1 model, this AM particle exposure model showed that MWCNT was bioactive and that nitrogen-doping significantly attenuated this bioactivity.

WLL cell ex vivo *studies*

Prior to full *in vivo* exposure studies, a 1-week *in vivo* particle exposure (50 μg) followed by lung cell removal and culture (*ex vivo*) with LPS (NF-κB activator) for 24 hr was done to determine if the NLRP3 inflammasome in the AM from the exposed mouse lungs were activated *in vivo*. Two cytokines associated with NLRP3 inflammasome activation were examined (IL-1β and IL-18), along with IL-33. The results from the *ex vivo* cultures can be found in Figure 8 (panels A–C). In all cases, the lung cells from MWCNT-exposed mice demonstrated significant changes in the release of the three cytokines. With IL-1β and IL-18 (Figure 8, panel A and B) there were significant increases associated with MWCNT exposure. In contrast, there was a significant decrease in IL-33 in the same exposure group (Figure 8, panel C). The NDMWCNT-exposed mice lung cells also showed increased IL-1β and IL-18, but it was significantly lower than the cells exposed to MWCNT. The IL-33 levels were not affected by NDMWCNT exposure. These results were consistent with the *in vitro* assessments that described the NDMWCNT as less bioactive than MWCNT.

In vivo *pulmonary inflammation and damage after exposure to NDMWCNT and MWCNT*

Pulmonary inflammation was assessed by determining WLL polymorphonuclear leukocytes (PMNs) in NDMWCNT-induced dose-dependent pulmonary inflammation at 1 and 7 days post-exposure (Figure 9, panel A). In addition, at the 40 μg dose of NDMWCNT, PMNs at 7 days post-exposure were significantly increased compared to the 1 day post-exposure (Figure 9, panel A). Comparison of mice exposed to 40 μg of NDMWCNT or MWCNT determined that NDMWCNT caused significantly less pulmonary inflammation at both 1 and 7 days post-exposure (Figure 9, panel B). Thus, NDMWCNT caused dose-dependent pulmonary inflammation, but on an equivalent mass basis it was less than that caused by MWCNT.

In vivo *NDMWCNT and MWCNT induced activation of the NLRP3 inflammasome*

To determine and compare activation of the NLRP3 inflammasome one day after exposure to NDMWCNT and MWCNT, phagolysosomal lysis was assessed by determining cathepsin activity and *in vivo* activation of the NLRP3 inflammasome by the cytokines IL-1β and IL-18 in first WLL fluid. In comparison to vehicle (DM)-exposed mice, exposure to NDMWCNT and MWCNT resulted in a significant elevation of total cathepsin activity (Figure 10, panel A). Total cathepsin activity in mice exposed to NDMWCNT was significantly lower than MWCNT-exposed mice. In regards to WLL fluid cytokines, mice exposed to either NDMWCNT or MWCNT had higher levels of IL-1β (Figure 10, panel B) and IL-18 (Figure 10, panel C) in comparison to DM-exposed mice. Comparison of the two particle exposed groups showed that NDMWCNT caused significantly less secretion of both IL-1β (Figure 10, panel B) and IL-18 (Figure 10, panel C) in comparison to MWCNT. These data indicate that both NDMWCNT and MWCNT caused phagolysosomal lysis and activation of the NLRP3 inflammasome, but these responses were significantly less for NDMWCNT in comparison to MWCNT.

Histopathology

Male C57 mice were exposed to either MWCNT, NDMWCNT or vehicle by pharyngeal aspiration and sacrificed at 7 and 56 days post exposure for evaluation of lung inflammation and fibrosis. Histopathology scores for inflammation and fibrosis are summarized in Tables 1 and 2. At 7 days post-exposure, inflammation and granuloma formation were seen following exposure to both particles (Figure 11, panels A–D). Inflammatory infiltrates were composed primarily of macrophages and fewer neutrophils, and were centered at the terminal bronchiole with extension into the alveolar duct and alveoli (Figure 11, Panels A and C). The number of animals affected and severity scores for inflammation were higher at 7 days following exposure to MWCNT compared to NDMWCNT, but were similar at 56 days. Black, spicule-like foreign material was frequently seen within inflammatory macrophages and associated with granulomas (Figure 11, panels B and D).

By 56 days post-exposure, the severity of pulmonary inflammation was greatly reduced with both particles (Figure 12, Panels A and C) compared to 7 days (Figure 11(A, C)). Scattered granulomas containing large deposits of particles (Figure 12, Panels B and D) were also seen at 56 days post-exposure with both MWCNT and NDMWCNT exposures. There were no treatment related abnormalities in lungs of vehicle-exposed mice at either time point (Figures 11 and 12, Panels E and F).

Fibrosis developed rapidly with exposure to both particles, and was observed within foci of inflammation and associated with granulomas following exposure at both time points (Figures 13 and 14). However, at 7 days post-exposure, the incidence and severity of these changes were higher following exposure to MWCNT compared to NDMWCNT. Interstitial fibrosis persisted at 56 days post-exposure with both particles, as evidenced by slight thickening of the alveolar walls by collagen on Picrosirius red staining.

Discussion

Previous studies in our laboratory have determined that post-synthesis surface modification of titanium dioxide nanoparticles (Hamilton et al. 2014) and MWCNT (Hamilton, Xiang, et al. 2013; Sager et al. 2014) change their respective bioactivity. In contrast, surface modification, i.e. doping, which is the incorporation of a heteroatom into the MWCNT structure during synthesis, has been shown to alter MWCNT crystallinity and reactivity properties that are important for industrial applications and may also alter their bioactivity, but this hypothesis has not been tested. Thus, in this study we compared the bioactivity of NDMWCNT and compared it to MWCNT to test the hypothesis that nitrogen doping would alter carbon nanotube bioactivity.

First, significant effort was invested in the characterization of the nanoparticles to aid interpretation of the outcomes of the *in vitro* and *in vivo* studies. HRTEM analyses determined that both NDMWCNT and MWCNT had distinctive multilayer structure that is characteristic of carbon nanotubes, and that the average layer distance was not changed by nitrogen doping.

Fiber length can be an important determinate of bioactivity, with increasing length being associated with more severe effects (Poland et al. 2008; Donaldson and Poland 2013; Hamilton, Xiang, et al. 2013). Thus, it was important to characterize the physical characteristics of NDMWCNT, and compare it to MWCNT. NDMWCNT width and length distributions were log normal, with count median length determined to be 4.73 μm (GSD 2.33) and count median width 52.6 nm (GSD 1.44). This is similar to MWCNT, which our laboratory previously reported to have a MWCNT median length of 3.86 μm (GSD 1.94) and count mean width of 49 nm (Porter et al. 2010). Given the similarity of physical parameters for NDMWCNT and MWCNT, differences in their bioactivity cannot be ascribed to differences in particle width and length.

Surface characteristics of both nanoparticles were investigated with XPS. Specifically, the XPS detailed scan of NDMWCNT showed a graphite-like ring structure with trace levels of carbon in the form of C–O, and nitrogen associated peaks ascribed to the O–C–N or the −C–NH_2 bonds. The XPS detailed scan of MWCNT was similar to NDMWCNT, except no nitrogen-associated peaks were detected. Taken together, the particle sizing data and XPS data indicate the two nanoparticles have similar physical parameters (length and width), and the functional groups on their surface are also similar, with the exception of the nitrogen functional groups of the NDMWCNT. Zeta potentials in DM were also similar, being −29.2 mv for NDMWCNT and −35.8 mV for MWCNT, which are consistent with functional groups identified on the surface of the samples by XPS.

The NDMWCNT and MWCNT in this study were in aqueous suspension prior to aspiration exposure. The hydrodynamic diameter of the NDMWCNT and MWCNT were similar, being 1.01 and 1.76 μm respectively, indicating the structures were not significantly different in size and were respirable. This avoided a complication previously reported in a rat IT study of single walled carbon nanotubes (SWCNT), where substantial agglomeration resulted in a

mortality rate of approximately 15% within 24 h post-exposure due to large SWCNT agglomerates blocking upper airways (Warheit et al. 2003).

Before conducting any *in vivo* studies, *in vitro* studies were conducted to assess if nitrogen doping impacted MWCNT bioactivity. Indeed, the THP-1 and mouse AM studies indicated nitrogen-doping of MWCNT decreased its bioactivity relative to MWCNT. This finding is consistent with an earlier report from our laboratory that showed MWCNT-exposed small airway epithelial cells had elevated cytotoxicity and cell proliferation in comparison to NDMWCNT-exposed cells (Mihalchik et al. 2015). In addition, the *in vitro* studies showed increased expression of IL-1β in MWCNT-exposed cells which mirrored the finding observed in the *ex vivo* AM study.

A previous study from our laboratory determined that inhaled MWCNT cause acute changes in lung function, and effects of NDMWCNT are less in comparison to MWCNT (Russ et al. 2019). In the present *in vivo* studies, NDMWCNT-induced pulmonary inflammation was assessed from PMN responses and was dose-dependent at both 1 and 7 days post-exposure. At 1 day post-exposure, the PMN response was greater than that at 7 days post-exposure, except at the 40 μg dose, where the response at 7 days post-exposure was greater than that at 1 day post-exposure. This is similar to the results obtained with MWCNT, which showed that response to 40 μg MWCNT peaked at 7 days post-exposure, and then decreased with post-exposure time (Porter et al. 2010). Comparison of equivalent 40 μg mass doses showed that at 1 and 7 days post-exposure NDMWCNT were less inflammatory than MWCNT. These data are supported by histopathology examination, which determined that inflammation tended to be more severe following exposure to MWCNT than NDMWCNT at 7 days post-exposure. Pulmonary fibrosis was minimal for both particles, but the incidence was much higher for MWCNT-exposed mice.

During the AM-mediated phagocytic process, vacuoles containing engulfed particles fuze with lysosomes, to form the phagolysosome. However, some particles damage the phagolysosome, causing its contents to leak, and these include several isoforms of cathepsin. The release of cathepsin B initiates activation of the NLRP3 inflammasome, which converts inactive pro forms of IL-1β and IL-18 to bioactive forms of these cytokines. They are subsequently secreted into the alveolar lining fluid promoting inflammation and fibrosis (Cassel et al. 2009). A previous study from our laboratory reported multi-walled carbon nanotubes induced elevated expression of several pro-inflammatory cytokines including IL-1β in lung tissues and lung lavage fluid in a dose- and time-dependent manner (Dong et al. 2015), suggesting activation of the NLRP3 inflammasome. In another study, we reported surface modification of MWCNT with −COOH group significantly reduced both activation of the NLRP3 inflammasome, evidenced by decreased cytokine levels and cathepsin activities in lung lavage fluid, and less severe lung fibrosis (Sager et al. 2014).

Increased levels of IL-1β after exposure to MWCNT and NDMWCNT in the *in vitro* and *ex vivo* studies suggested that phagolysosomal permeabilization and activation of the NLRP3 inflammasome should be examined *in vivo*. Indeed, cathepsin activity in WLL fluid was increased in NDMWCNT-exposed mice versus vehicle controls, whereas cathepsin activity in WLL fluid from MWCNT-exposed mice had even higher activities. Furthermore, IL-1β

and IL-18 levels in WLL fluid followed a similar pattern. Taken together, these data indicate that *in vivo* NDMWCT cause phagolysosomal lysis and subsequent activation of the NLRP3 inflammasome, but that the extent is less that that caused by MWCNT exposure.

Length, aspect ratio and particle rigidity has been shown to affect activation of the NLRP3 inflammasome (Palomaki et al. 2011). Subsequently, our laboratory extended these findings by demonstrating surface modification of MWCNT with −COOH group significantly reduced activation of the NLRP3 inflammasome (Sager et al. 2014). In the present study, we demonstrated nitrogen doping of MWCNT resulted in lower activation of the NLRP3 inflammasome relative to MWCNT. However, the underlying mechanism responsible for differential activation of the NLRP3 inflammasome remains to be determined. Other studies have suggested that lysosomal membrane permeability may be the key underlying regulator of particle-induced inflammation leading to fibrosis (Biswas et al. 2017). To address this knowledge gap, our research team is investigating how bioactive nanoparticles alter membrane permeability of the phagolysosome, leading to cathepsin release and subsequent NLRP3 inflammasome activation.

Our laboratory has reported that MWCNT exposure promotes the growth and neoplastic progression of initiated lung cells in B6C3F1 mice (Sargent et al. 2014). Cell proliferation and inflammation are important events in the promotion of cancer (Pitot et al. 1989; Pitot 1993; Malkinson 2004; Bauer et al. 2005; Hussain and Harris 2007; Bauer and Rondini 2009). We have previously reported that MWCNT-exposed small airway epithelial cells demonstrated elevated cytotoxicity and cell proliferation in comparison to NDMWCNT-exposed cells (Mihalchik et al. 2015). In the present study, we report NDMWCNT exposure results in less lung inflammation than that caused by MWCNT. In addition, our laboratory recently published a study which showed that in comparison to MWCNT, NDMWCNT caused a lower incidence of genotoxicity, although the type of mitotic and chromosome aberrations was similar (Siegrist et al. 2019). Taken together, these studies suggest nitrogen doping of MWCNT reduces the risk of lung fibrosis in exposed workers, and advances the hypothesis that nitrogen doping of MWCNT may also reduce MWCNT carcinogenic potential. This hypothesis is currently being tested using an initiation-promotion model in a B6C3F1 *in vivo* mouse model.

Acknowledgements

The authors would like to thank Phillip Brown (NIOSH) for the editorial review of the manuscript.

Abbreviations:

NDMWCNT	nitrogen-doped multi-walled carbon nanotubes
MWCNT	multi-walled carbon nanotubes
TEM	transmission electron microscopy
HRTEM	high resolution transmission electron microscopy
IL-1ß	interleukin-1ß

DM	dispersion medium
WLL	whole lung lavage
IL-18	interleukin-18
GSD	geometric standard deviation
XPS	X-ray photoelectron spectroscopy
SEM	standard error of the mean
PMA	phorbol 12-myristate 13-acetate
LPS	lipopolysacharride
LDH	lactate dehydrogenase
AM	alveolar macrophage
PMN	polymorphonuclear leukocyte

References

Bauer AK, Dixon D, DeGraff LM, Cho HY, Walker CR, Malkinson AM, Kleeberger SR. 2005 Toll-like receptor 4 in butylated hydroxy-toluene-induced mouse pulmonary inflammation and tumorigenesis. J Natl Cancer Inst. 97(23):1778–1781. [PubMed: 16333033]

Bauer AK, Rondini EA. 2009 Review paper: the role of inflammation in mouse pulmonary neoplasia. Vet Pathol. 46(3):369–390. [PubMed: 19176494]

Biswas R, Trout KL, Jessop F, Harkema JR, Holian A. 2017 Imipramine blocks acute silicosis in a mouse model. Part Fibre Toxicol. 14(1):36. [PubMed: 28893276]

Cassel SL, Joly S, Sutterwala FS. 2009 The NLRP3 inflammasome: a sensor of immune danger signals. Semin Immunol. 21(4):194–198. [PubMed: 19501527]

Dahm MM, Evans DE, Schubauer-Berigan MK, Birch ME, Fernback JE. 2012 Occupational exposure assessment in carbon nanotube and nanofiber primary and secondary manufacturers. Ann Occup Hyg. 56(5):542–556. [PubMed: 22156567]

Donaldson K, Poland CA. 2013 Nanotoxicity: challenging the myth of nano-specific toxicity. Curr Opin Biotechnol. 24(4):724–734. [PubMed: 23768801]

Dong J, Porter DW, Batteli LA, Wolfarth MG, Richardson DL, Ma Q. 2015 Pathologic and molecular profiling of rapid-onset fibrosis and inflammation induced by multi-walled carbon nanotubes. Arch Toxicol. 89(4):621–633. [PubMed: 25510677]

Dostert C, Petrilli V, Van Bruggen R, Steele C, Mossman BT, Tschopp J. 2008 Innate immune activation through Nalp3 inflammasome sensing of asbestos and silica. Science. 320(5876):674–677. [PubMed: 18403674]

Hamilton RF Jr., Wu Z, Mitra S, Shaw PK, Holian A. 2013 Effect of MWCNT size, carboxylation, and purification on in vitro and in vivo toxicity, inflammation and lung pathology. Part Fibre Toxicol. 10(1):57. [PubMed: 24225053]

Hamilton RF, Wu N, Xiang C, Li M, Yang F, Wolfarth M, Porter DW, Holian A. 2014 Synthesis, characterization, and bioactivity of carboxylic acid-functionalized titanium dioxide nanobelts. Part Fibre Toxicol. 11:43. [PubMed: 25179214]

Hamilton RF Jr., Xiang C, Li M, Ka I, Yang F, Ma D, Porter DW, Wu N, Holian A. 2013 Purification and sidewall functionalization of multiwalled carbon nanotubes and resulting bioactivity in two macrophage models. Inhal Toxicol. 25(4):199–210. [PubMed: 23480196]

Han JH, Lee EJ, Lee JH, So KP, Lee YH, Bae GN, Lee SB, Ji JH, Cho MH, Yu IJ. 2008 Monitoring multiwalled carbon nanotube exposure in carbon nanotube research facility. Inhal Toxicol. 20(8): 741–749. [PubMed: 18569096]

Hussain SP, Harris CC. 2007 Inflammation and cancer: an ancient link with novel potentials. Int J Cancer. 121(11):2373–2380. [PubMed: 17893866]

Kim YA, Hayashi T, Endo M, Kaburagi Y, Tsukada T, Shan J, Osato K, Tsuruoka S. 2005 Synthesis and structural characterization of thin multi-walled carbon nanotubes with a partially facetted cross section by a floating reactant method. Carbon. 43(11):2243–2250.

Lee JH, Lee SB, Bae GN, Jeon KS, Yoon JU, Ji JH, Sung JH, Lee BG, Lee JH, Yang JS, et al. 2010 Exposure assessment of carbon nanotube manufacturing workplaces. Inhal Toxicol. 22(5):369–381. [PubMed: 20121582]

Li RB, Wang X, Ji ZX, Sun BB, Zhang HY, Chang CH, Lin SJ, Meng H, Liao YP, Wang MY, et al. 2013 Surface charge and cellular processing of covalently functionalized multiwall carbon nanotubes determine pulmonary toxicity. Acs Na. 7(3):2352–2368.

Malkinson AM. 2004 Role of inflammation in mouse lung tumorigenesis: a review. Exp Lung Res. 31(1):57–82.

Maynard AD, Baron PA, Foley M, Shvedova AA, Kisin ER, Castranova V. 2004 Exposure to carbon nanotube material: Aerosol release during the handling of unrefined single-walled carbon nanotube material. J Toxicol Env Heal A. 67(1):87–107.

Mihalchik AL, Ding W, Porter DW, McLoughlin C, Schwegler-Berry D, Sisler JD, Stefaniak AB, Snyder-Talkington BN, Cruz-Silva R, Terrones M, et al. 2015 Effects of nitrogen-doped multi-walled carbon nanotubes compared to pristine multi-walled carbon nanotubes on human small airway epithelial cells. Toxicology. 333:25–36. [PubMed: 25797581]

Palomaki J, Valimaki E, Sund J, Vippola M, Clausen PA, Jensen KA, Savolainen K, Matikainen S, Alenius H. 2011 Long, needle-like carbon nanotubes and asbestos activate the NLRP3 inflammasome through a similar mechanism. Acs Na. 5(9):6861–6870.

Pitot HC. 1993 Multistage carcinogenesis-genetic and epigenetic mechanisms in relation to cancer prevention. Cancer Detect Prev. 17(6):567–573. [PubMed: 8275509]

Pitot HC, Campbell HA, Maronpot R, Bawa N, Rizvi TA, Xu YH, Sargent L, Dragan Y, Pyron M. 1989 Critical parameters in the quantitation of the stages of initiation, promotion, and progression in one model of hepatocarcinogenesis in the rat. Toxicol Pathol. 17(4_part_1):594–611. discussion 611–592. [PubMed: 2697939]

Poland CA, Duffin R, Kinloch I, Maynard A, Wallace WA, Seaton A, Stone V, Brown S, Macnee W, Donaldson K. 2008 Carbon nanotubes introduced into the abdominal cavity of mice show asbestoslike pathogenicity in a pilot study. Nature Nanotech. 3(7):423–428.

Porter DW, Hubbs AF, Mercer RR, Wu N, Wolfarth MG, Sriram K, Leonard S, Battelli L, Schwegler-Berry D, Friend S. 2010 Mouse pulmonary dose- and time course-responses induced by exposure to multi-walled carbon nanotubes. Toxicology. 269(2–3):136–147. [PubMed: 19857541]

Porter D, Sriram K, Wolfarth M, Jefferson A, Schwegler-Berry D, Andrew M, Castranova V. 2008 A biocompatible medium for nanoparticle dispersion. Nanotoxicology. 2(3):144–154.

Russ KA, Thompson JA, Kashon M, Porter DW, Friend SA, McKinney W, Fedan JS. 2019 Comparison of multi-wall carbon nanotube and nitrogen-doped multi-wall carbon nanotube effects on lung function and airway reactivity in rats. Toxicol Appl Pharmacol. 364:153–163. [PubMed: 30423287]

Sager TM, Wolfarth MW, Andrew M, Hubbs A, Friend S, Chen TH, Porter DW, Wu NQ, Yang F, Hamilton RF, et al. 2014 Effect of multi-walled carbon nanotube surface modification on bioactivity in the C57BL/6 mouse model. Nanotoxicology. 8(3):317–327. [PubMed: 23432020]

Sargent LM, Porter DW, Staska LM, Hubbs AF, Lowry DT, Battelli L, Siegrist KJ, Kashon ML, Mercer RR, Bauer AK, et al. 2014 Promotion of lung adenocarcinoma following inhalation exposure to multi-walled carbon nanotubes. Part Fibre Toxicol. 11(1):3. [PubMed: 24405760]

Siegrist KJ, Reynolds SH, Porter DW, Mercer RR, Bauer AK, Lowry D, Cena L, Stueckle T A, Kashon M L, Wiley J, et al. 2019 Mitsui-7, heat-treated, and nitrogen-doped multi-walled carbon nanotubes elicit genotoxicity in human lung epithelial cells. Part Fibre Toxicol. 16(1):36. [PubMed: 31590690]

Tong H, McGee JK, Saxena RK, Kodavanti UP, Devlin RB, Gilmour MI. 2009 Influence of acid functionalization on the cardiopulmonary toxicity of carbon nanotubes and carbon black particles in mice. Toxicol Appl Pharmacol. 239(3):224–232. [PubMed: 19481103]

Warheit DB, Laurence BR, Reed KL, Roach DH, Reynolds GA, Webb TR. 2003 Comparative pulmonary toxicity assessment of single-wall carbon nanotubes in rats. Toxicol Sci. 77(1):117–125. [PubMed: 14514968]

WTEC Panel Report on Nanotechnology Research Directions for Societal Needs in 2020 Retrospective and Outlook. 2010.

Yang WR, Thordarson P, Gooding JJ, Ringer SP, Braet F. 2007 Carbon nanotubes for biological and biomedical applications. Nanotechnology. 18(41):412001.

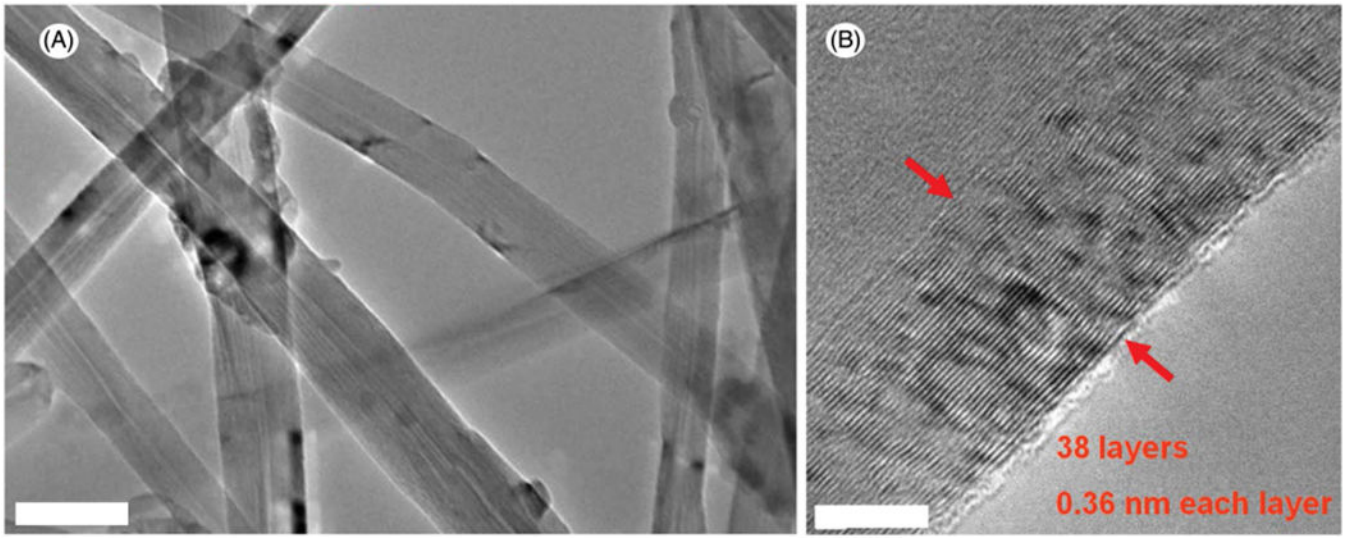

Figure 1.
Image of MWCNT. (A) low-magnification TEM, scale bar: 100 nm; (B) high-resolution TEM, scale bar: 2 nm.

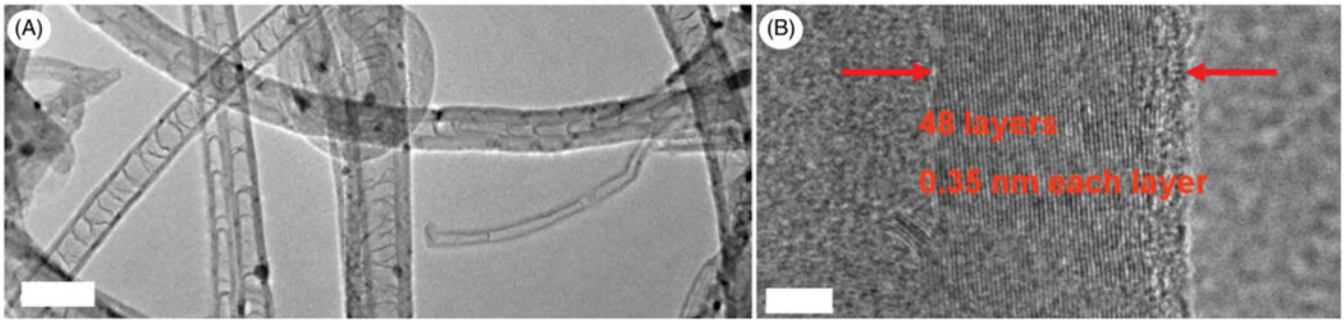

Figure 2.
Image of NDMWCNT. (A) low-magnification TEM, scale bar: 100 nm; (B) high-resolution TEM, scale bar: 5 nm.

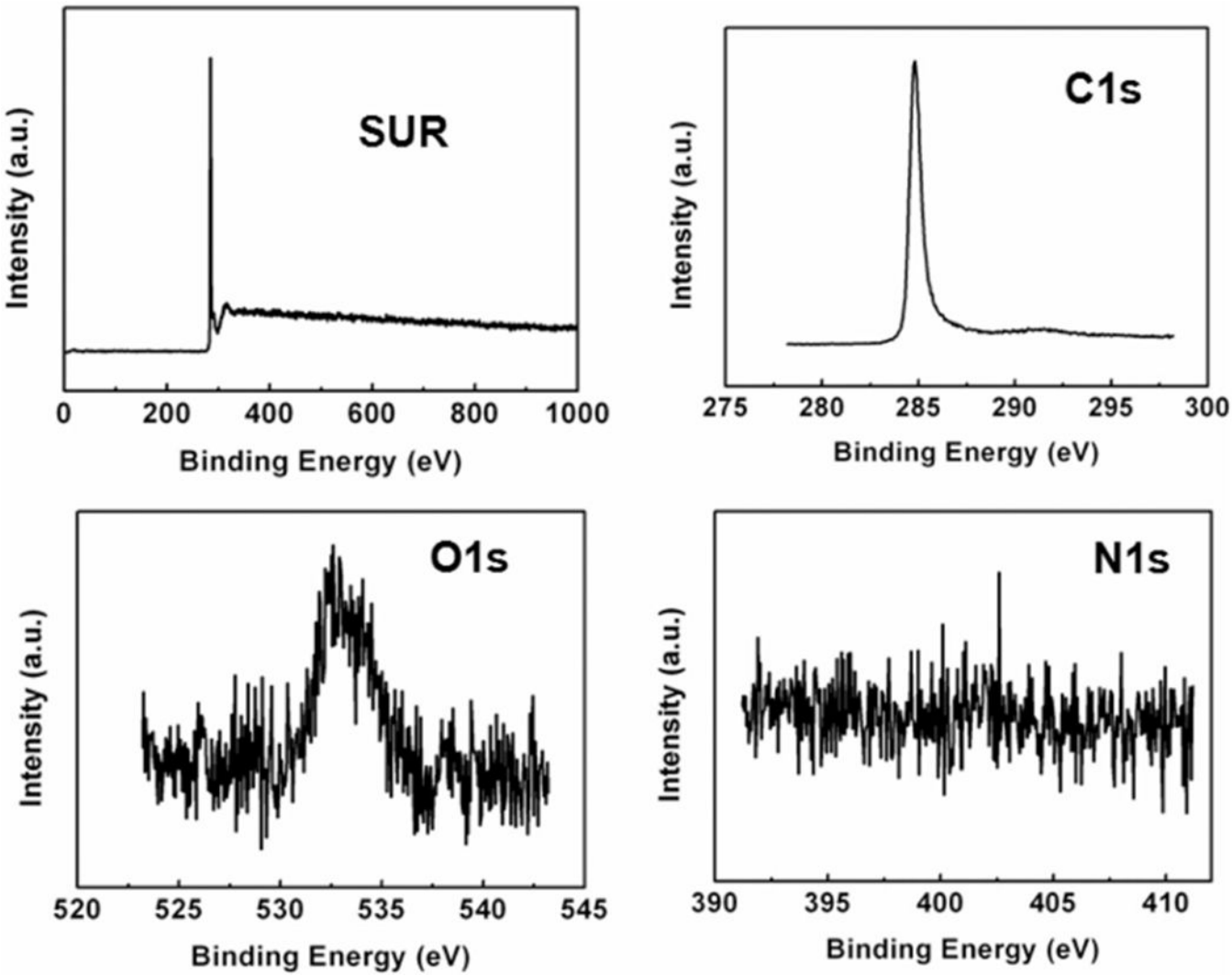

Figure 3.

XPS spectra of MWCNT including the survey scan and the detailed cans of C 1 s, O 1 s and N 1 s core-levels.

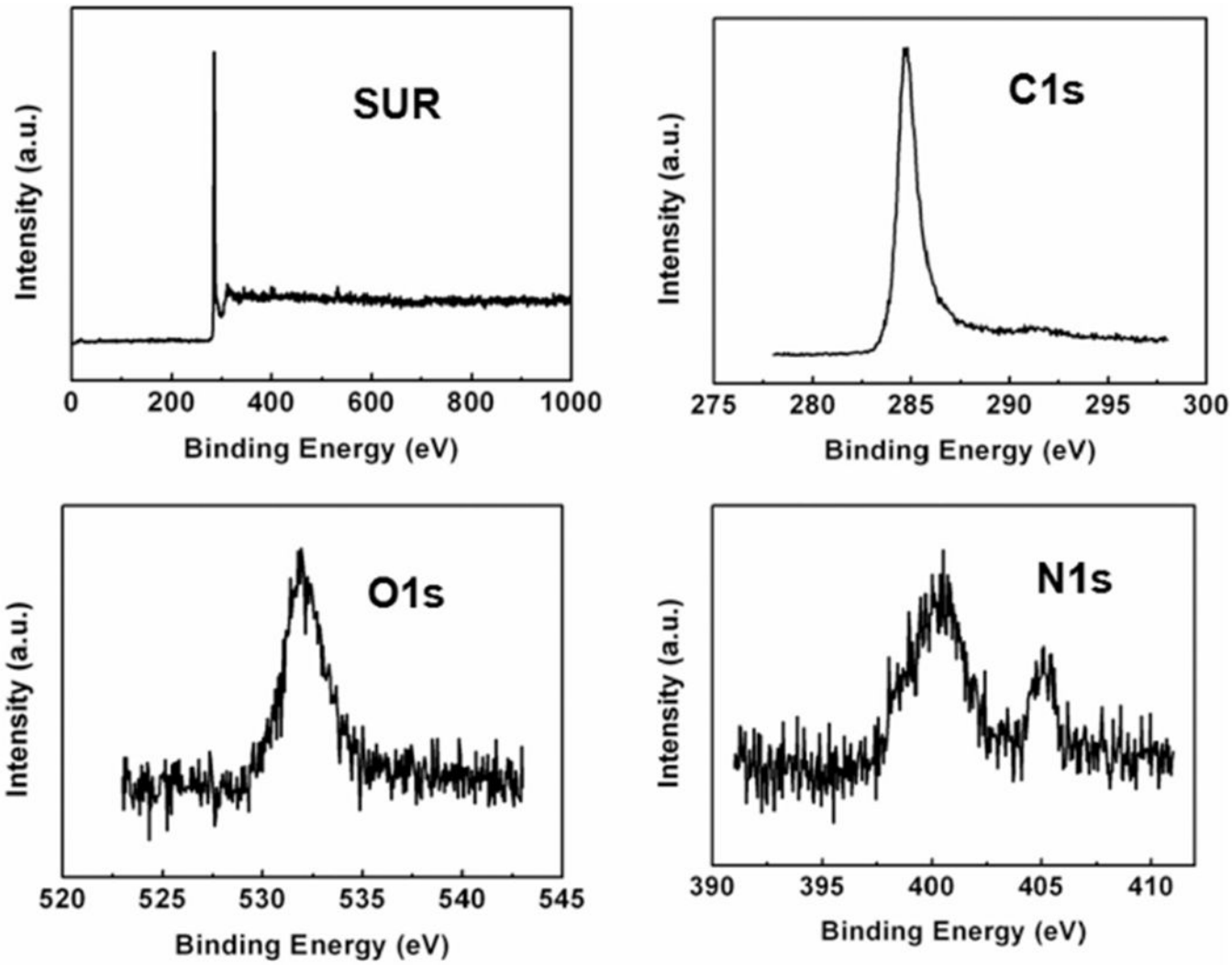

Figure 4.
XPS spectra of NDMWCNT including the survey scan and the detailed cans of C 1s, O 1s and N 1s core-levels.

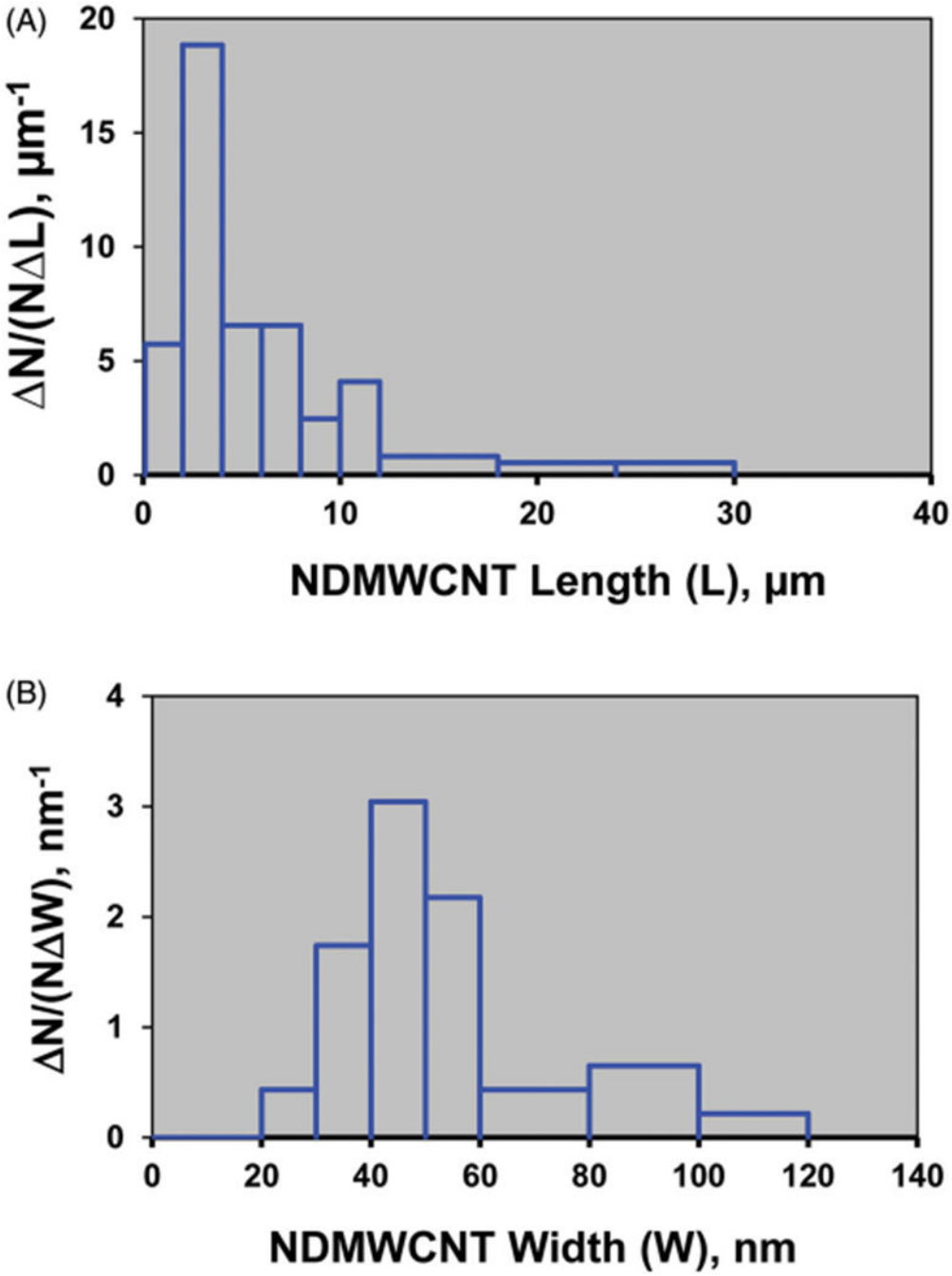

Figure 5.

Length and width size distribution of a hydrosol of NDMWCNT. The NDMWCNT length distribution had a count median length of 4.73 μm (GSD 2.33) (A) and count median width distribution of 52.6 nm (GSD 1.44) (B).

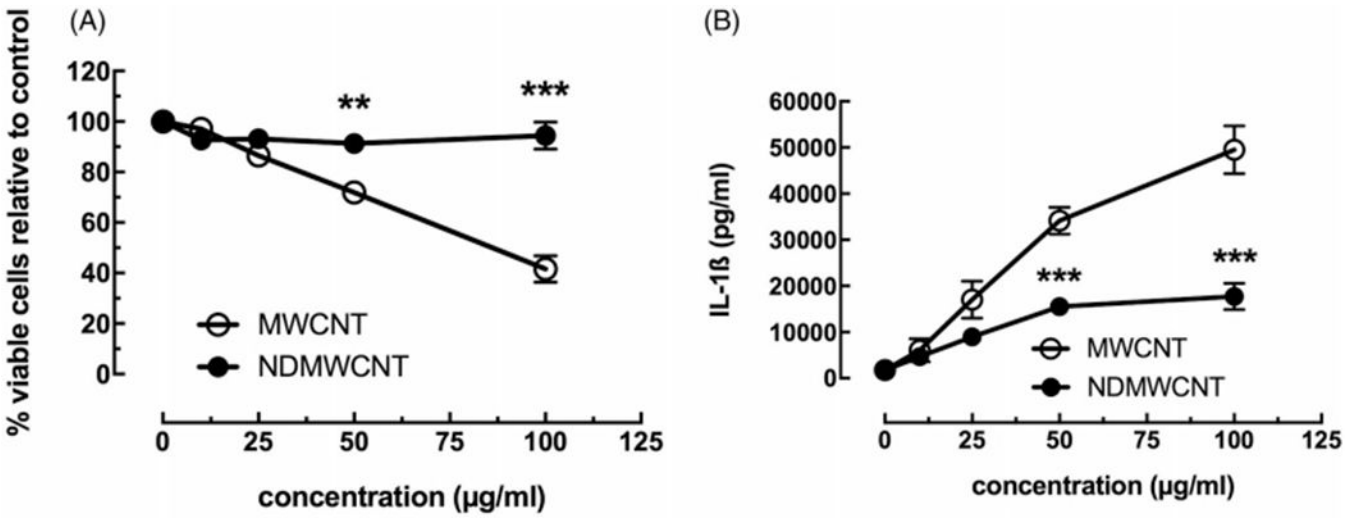

Figure 6.

In vitro toxicity and NLRP3 inflammasome activation due to MWCNT and NDMWCNT (0, 12.5, 25, 50 and 100 µg/ml) from transformed THP-1 macrophage-like cells in 24 hr culture. Data expressed as mean ± SEM. (A) MTS assay performed on cells 24 hr post-exposure. (B) NLRP3 inflammasome activation as measured by IL-1β release from cell culture 24 hr post-particle exposure. Asterisks *** indicates $p<0.001$ or ** $p<0.01$ compared to corresponding NDMWCNT dose. $n = 3$ to 4 experimental replications.

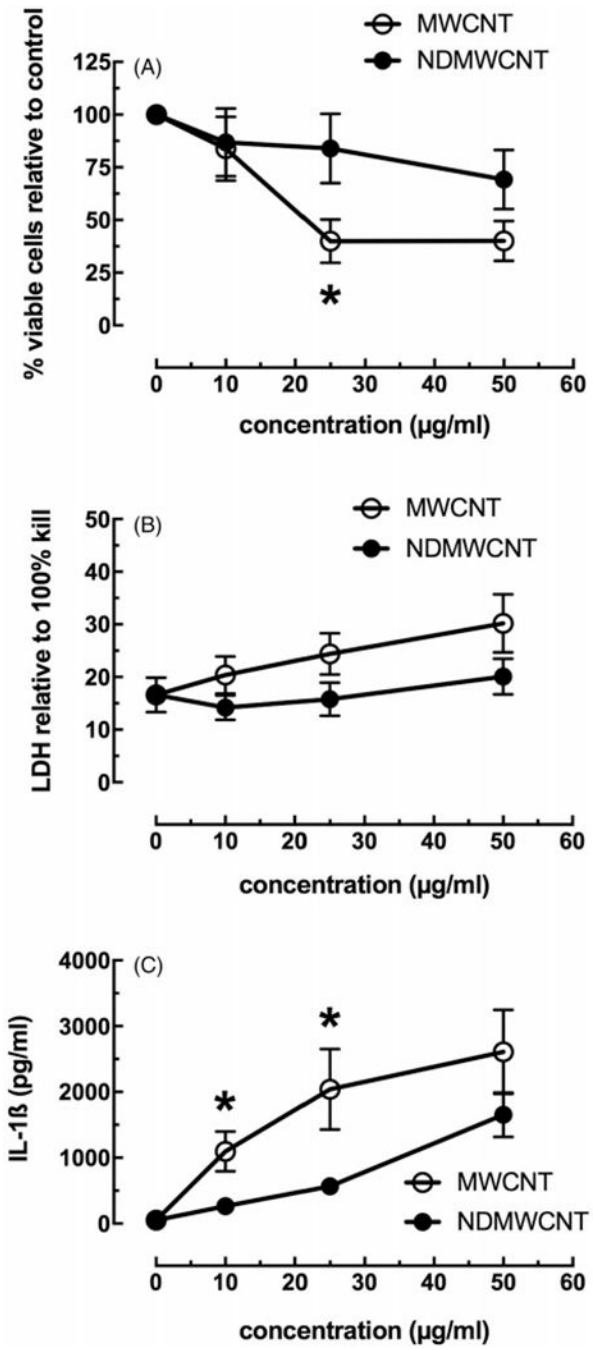

Figure 7.

In vitro toxicity and NLRP3 inflammasome activation to MWCNT and NDMWCNT (0, 10, 25 and 50 μg/mL) from isolated AM in 24 hr culture. Data expressed as mean ± SEM. (A) MTS assay performed on cells 24 hr post-exposure. (B) LDH assay performed on isolated culture media from 24 hr post-exposure cultures. Data relative to 100% cell lysis. (C) NLRP3 inflammasome activation as measured by IL-1β release from cell culture 24 hr post-particle exposure. Asterisk * indicates $p<0.05$ compared to corresponding NDMWCNT dose. $n = 3$ to 4 experimental replications.

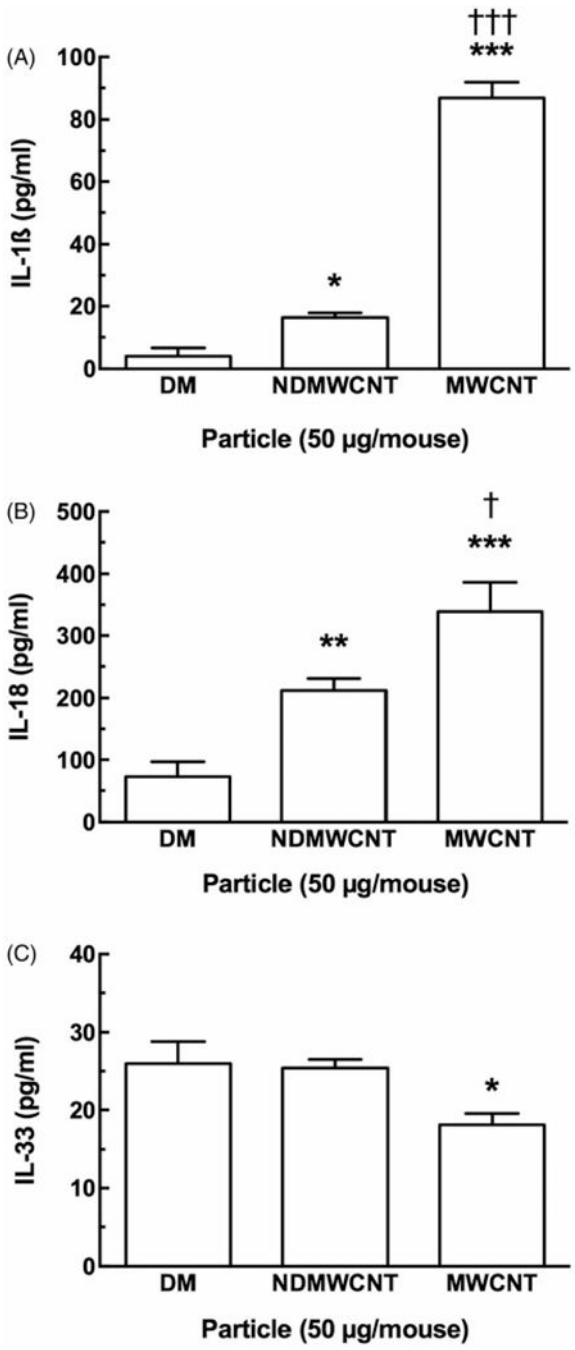

Figure 8.

Ex vivo cytokine release from isolated lung cells co-cultured with LPS (20ng/ml) for 24 hours. This cell isolation was from mice instilled with 50 µg of MWCNT variant or vehicle for 7 days previously. Data expressed as mean ± SEM. (A) IL-1β release from isolated lung cells. (B) IL-18 from isolated lung cells. (C) IL-33 from isolated lung cells. Asterisks *** indicate $p<0.001$ or *$p<0.05$ compared to vehicle control. One dagger † indicate $p<0.05$ compared to NDMWCNT condition. Daggers ††† indicate $p<0.001$ compared to NDMWCNT condition. $n = 8$ to 9 mice.

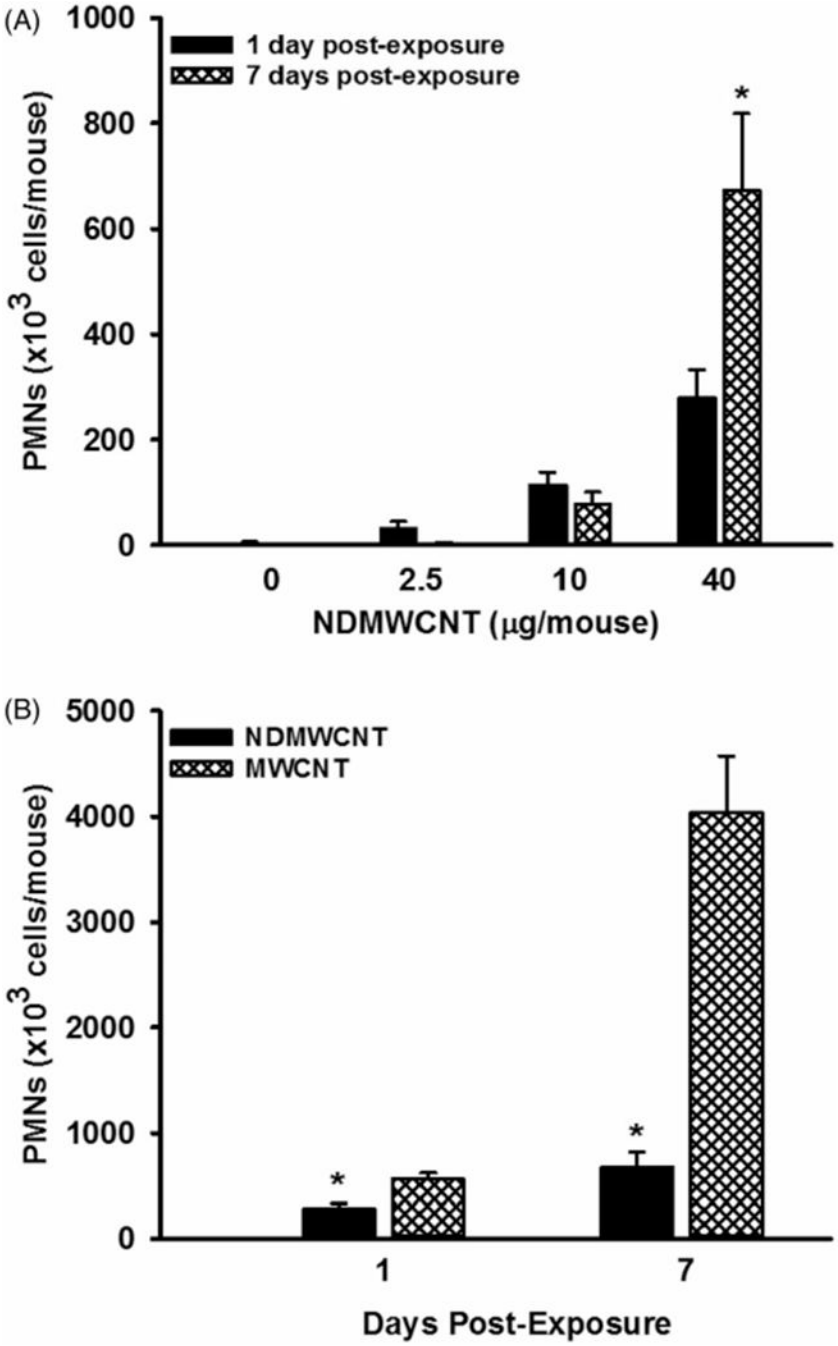

Figure 9.

Pulmonary inflammation induced by exposure to carbon nanotubes. Mice were exposed to DM, NDMWCNT (2.5 20 or 40 μg/mouse) or MWCNT (40 μg/mouse) and WLL studies were conducted at 1 and 7 days post-exposure. Pulmonary inflammation was assessed by determining WLL polymorphonuclear leukocytes. In Panel A, the dose-response and time course of NDMWCNT is shown. At a given dose, an asterisk (*) indicates a significant difference between 1 and 7 days post-exposure. In Panel B, comparison of pulmonary inflammation caused by exposure to 40 μg of NDMWCNT or MWCNT is shown. An

asterisk (*) indicates the NDMWCNT response was significantly lower ($p<0.05$) in comparison to the MWCNT exposed mice at the same post-exposure time. Values are means ±SEM ($n = 8$).

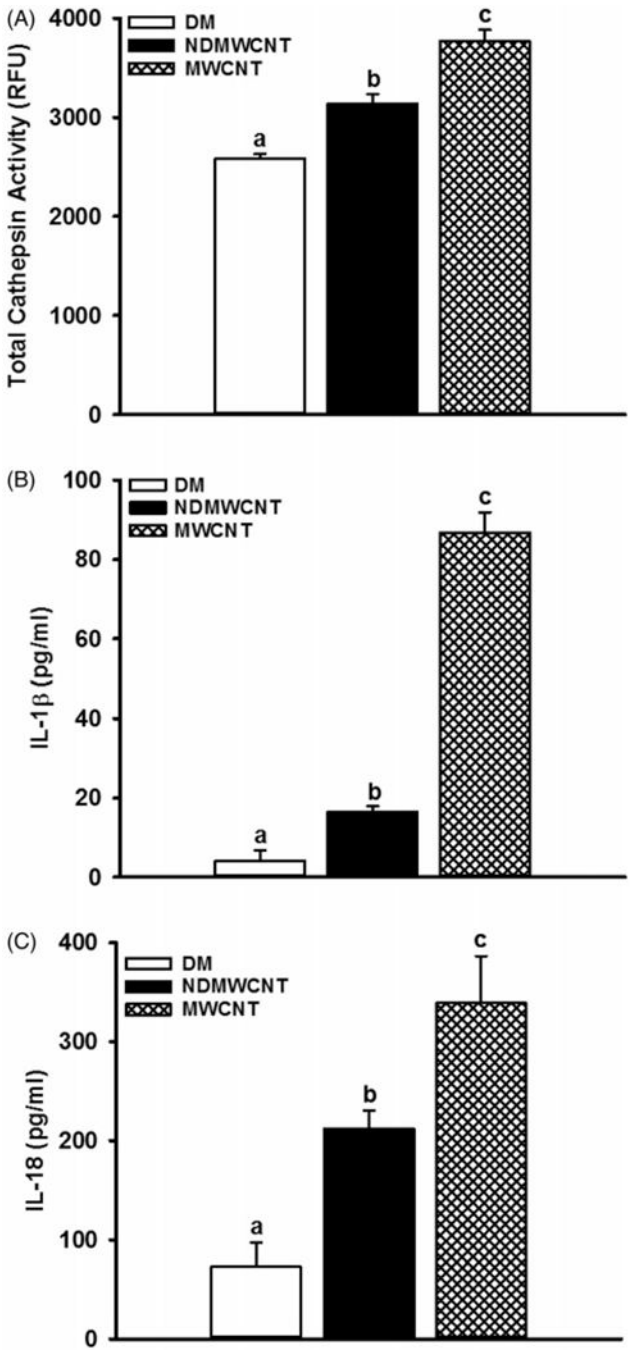

Figure 10.

Activation of the NLRP3 inflammasome. Mice were exposed to DM, NDMWCNT or MWCNT (40 μg/mouse) and WLL studies were conducted at 1 day post-exposure. Phagolysosomal lysis was assessed by determining cathepsin activity (panel A), while in first WLL fluid. The cytokines IL-1β (panel B) and IL-18 (panel C) were determined as markers of NLRP3 inflammasome activation. Values are means±SEM ($n = 8$). Bars with different letters are significantly different ($p<0.05$).

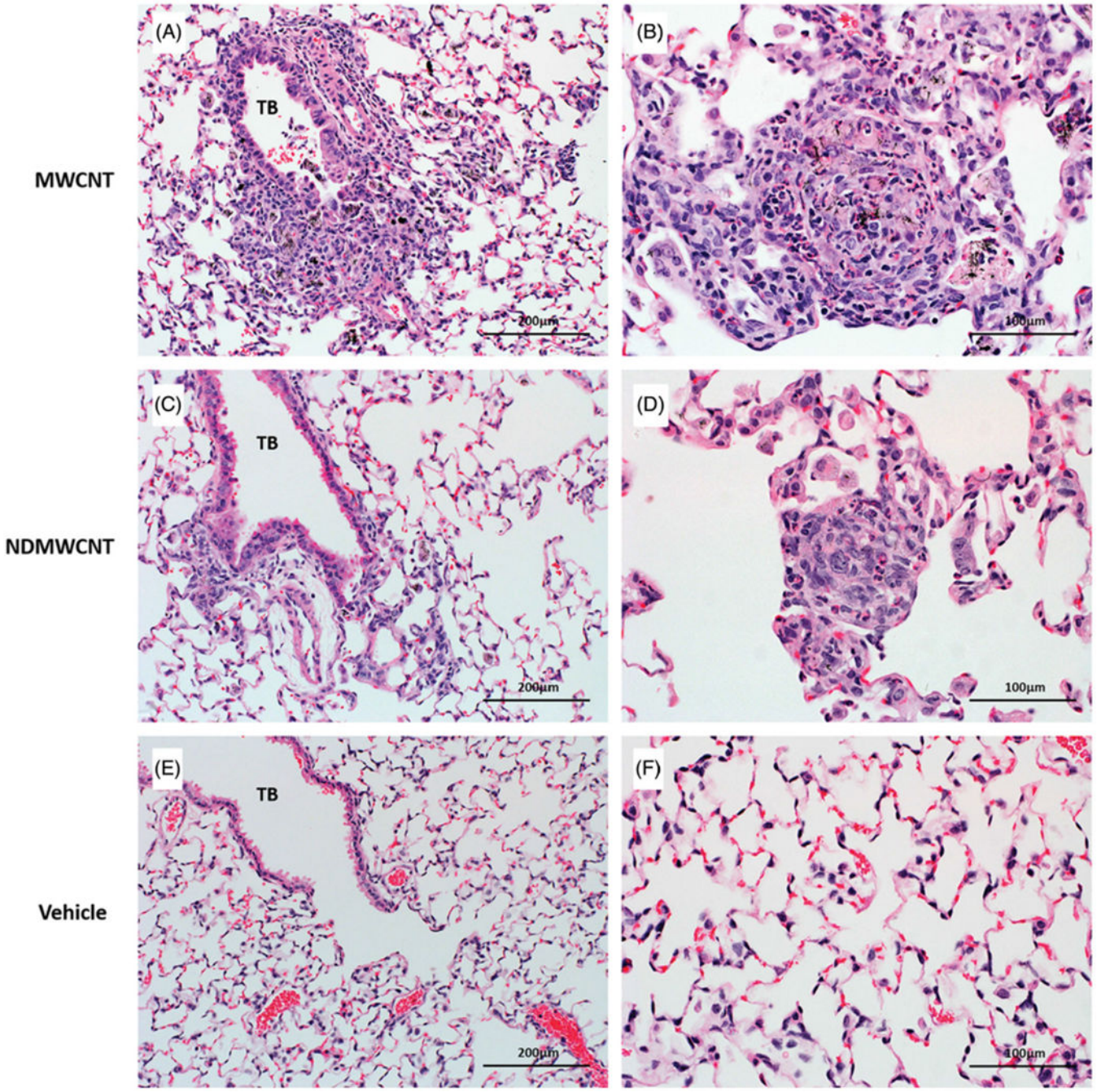

Figure 11.

Representative photomicrographs of murine lung at 7 days post exposure to MWCNT, NDMWCNT or DM. Inflammation at the terminal bronchiole (TB) (Panels A & C) and granuloma formation (Panels B & D) was seen following exposure to both particles. Normal lung anatomy was seen in lung of vehicle-exposed mice (Panels E & F).

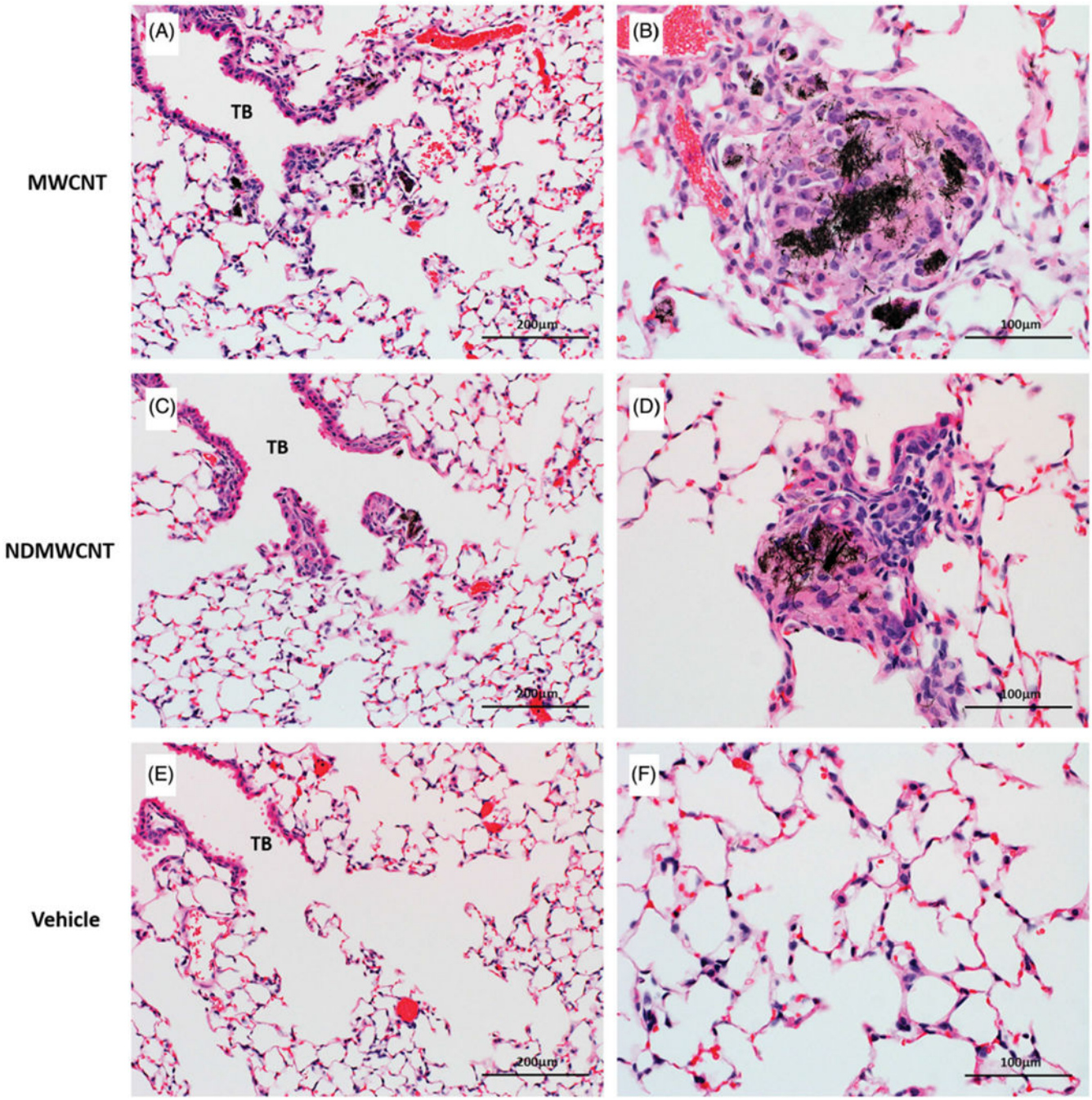

Figure 12.

Representative photomicrographs of murine lung at 56 days post exposure to MWCNT, NDMWCNT or DM. Inflammation at the terminal bronchioles (TB) is greatly reduced at 56 days (Panels A & C) when compared to 7 days. The centers of granulomas contain large numbers of black particles (Panels B & D) following exposure to both MWCNT and NDMWCNT. Normal lung anatomy was seen in lung of vehicle-exposed mice (Panels E & F).

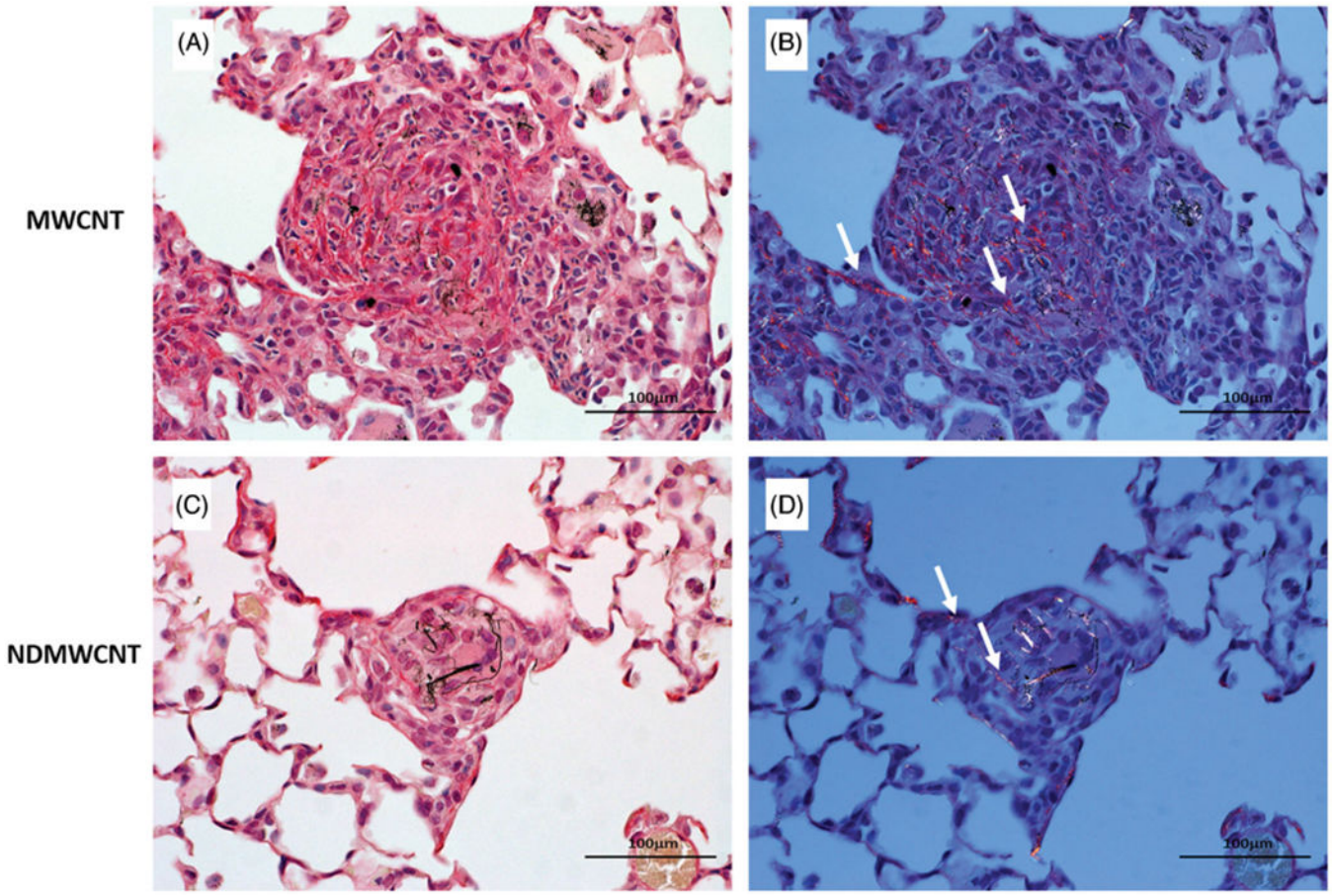

Figure 13.

Representative photomicrographs of murine lung at 7 days post exposure to MWCNT or NDMWCNT and stained with Sirius Red for evaluation of fibrosis. Stained sections were evaluated with bright field microscopy (Panels A & C) or with polarizing light microscopy (Panels B & D). Fibrosis is present within granulomas following exposure to both particles and appears red/orange with polarization (white arrows).

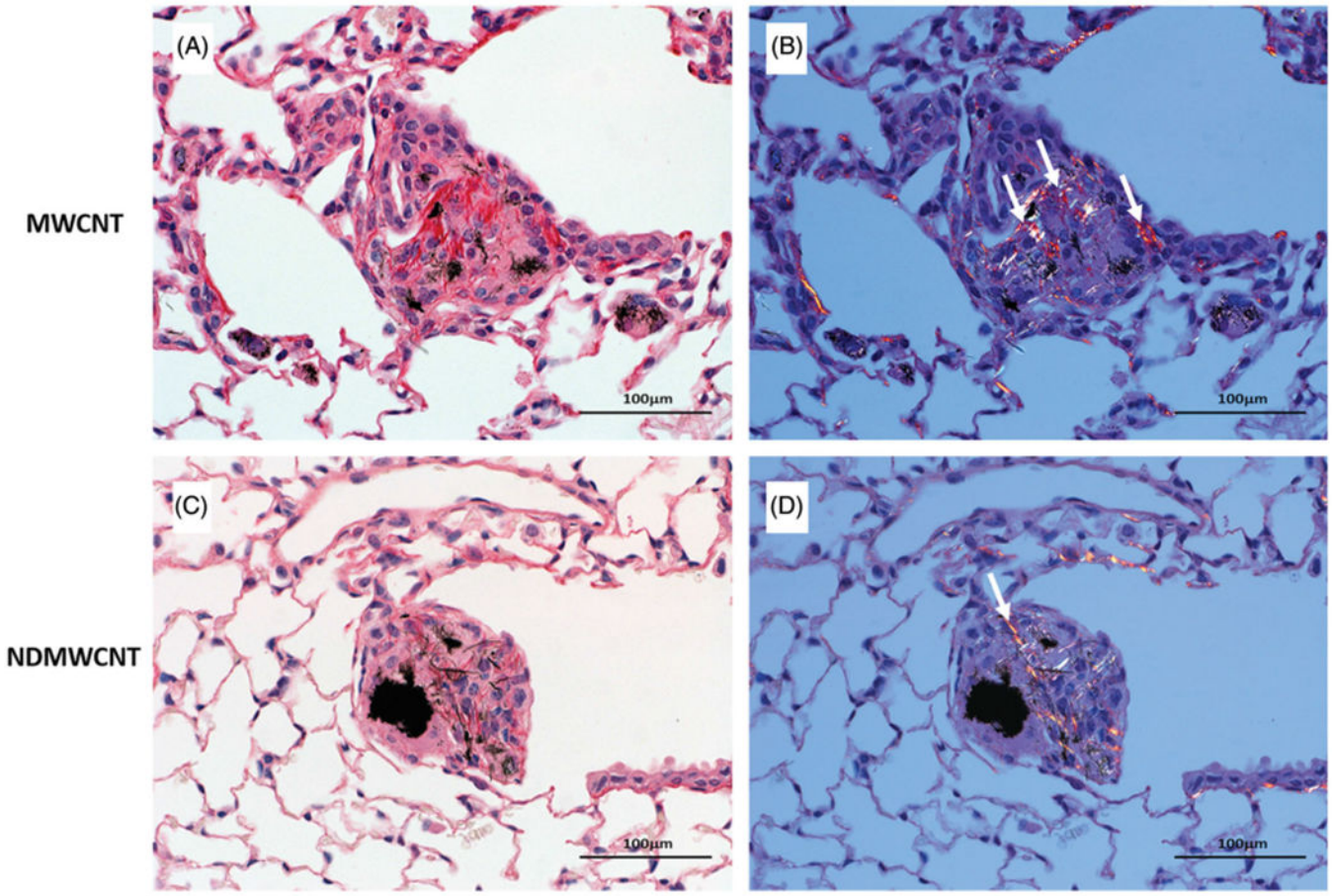

Figure 14.

Representative photomicrographs of murine lung at 56 days post exposure to MWCNT or NDMWCNT and stained with picrosirius red for evaluation of fibrosis. Stained sections were evaluated with bright-field microscopy (Panels A & C) or with polarizing light microscopy (Panels B & D). Fibrosis is present within granulomas following exposure to both particles and appears red/orange with polarization (white arrows).

Table 1.

Summary of histopathological findings of inflammation[a,b].

Treatment Group	Days Post-Exposure: 7		Days Post-Exposure: 56	
DM	0 (n=8)	A	0 (n=7) 2 (n=1)	A
NDMWCNT	0 (n=1) 4 (n=7)	B	2 (n=1) 4 (n=6)	B
MWCNT	4 (n=1) 5 (n=5) 6 (n=2)	C	4 (n=8)	B

[a]Values represent histopathology score and inside parentheses the number of animals (*n*) with that score.

[b]Treatment groups within the same post-exposure time with different letters are significantly different ($p < 0.05$).

Table 2.

Summary of histopathological findings of fibrosis[a,b].

Treatment Group	Days Post-Exposure 7		Days Post-Exposure 56	
DM	0 (n=8)	A	0 (n=8)	A
NDMWCNT	0 (n=5) 4 (n=3)	A	0 (n=1) 2 (n=2) 4 (n=4)	B
MWCNT	4 (n=8)	B	4 (n=8)	B

[a]Values represent histopathology score and inside parentheses the number of animals (*n*) with that score.

[b]Treatment groups within the same post-exposure time with different letters are significantly different ($p < 0.05$).